Novel Quantification of Real-Time Lymphatic Clearance: Immediate Lymphatic Reconstruction in a Large-Animal Model

Anna Rose Johnson, M.D., M.P.H.
Marc-André Tétrault, Ph.D.
Miguel G. Bravo, M.D.
Vincent Girouard, B.S.
Rita Laurence, B.S.
Bernard T. Lee, M.D., M.B.A., M.P.H.
Hak Soo Choi, Ph.D.
Dhruv Singhal, M.D.

Boston, Mass.

Background: The real-time quantification of lymphatic flow remains elusive. Efforts to provide a metric of direct lymphatic function are not clinically translatable and lack reproducibility. Early reports demonstrate the promise of immediate lymphatic reconstruction (immediate lymphovenous bypass after lymphadenectomy) to reduce the risk of lymphedema development. However, there remains a heightened need to appraise this technique in a clinically translatable large-animal model. The aim of the authors' experiment was to evaluate the role of molecular imaging in the quantification of real-time lymphatic flow after lymphadenectomy, and lymphadenectomy with lymphovenous bypass using novel fluorophores in a swine model.
Methods: A lymphadenectomy or lymphadenectomy with subsequent lymphovenous bypass was performed in 10 female swine. After subdermal fluorophore injection, near-infrared molecular imaging of blood samples was used to evaluate change in lymphatic flow after lymphadenectomy versus after lymphadenectomy with lymphovenous bypass. Continuous imaging evaluating fluorescence of the superficial epigastric vein in the torso and adjacent skin was performed throughout all experiments. Findings between modalities were correlated.
Results: The near-infrared dye signal in central and peripheral blood samples was often difficult to separate from background and proved challenging for reliable quantification. Venous and skin near-infrared imaging demonstrated a lymphatic clearance rate decrease of 70 percent after lymphadenectomy versus a decrease by only 30 percent after lymphadenectomy with immediate lymphovenous bypass.
Conclusions: In this article, the authors describe a noninvasive, swine, large-animal model to quantify lymphatic clearance using skin imaging. The authors' findings were consistent with results yielded from real-time imaging of the vein. The authors believe this model may have important implications for eventual direct translation to the clinical setting. (*Plast. Reconstr. Surg.* 149: 130, 2022.)

Despite tremendous advancements in the field of lymphatic surgery, there remains no reproducible, reliable, and objective modality that quantifies lymphatic flow in real time. This is problematic, as it precludes any ability to directly evaluate the efficacy of surgical and nonsurgical interventions for lymphedema and their impact on lymphatic function.

Efforts to evaluate real-time lymphatic clearance can be traced to the 1950s, with lymphoscintigraphy.[1] Quantitative lymphoscintigraphy emerged as a technique that provided the ability to quantify real-time lymphatic function. It directly calculates the rate of

From the Division of Plastic and Reconstructive Surgery, Beth Israel Deaconess Medical Center, Harvard Medical School; and Gordon Center for Molecular Imaging, Department of Radiology, Massachusetts General Hospital, Harvard Medical School.
Received for publication July 14, 2020; accepted June 21, 2021.
Presented at the 2020 American Society for Reconstructive Microsurgery Annual Meeting, in Fort Lauderdale, Florida, on January 11 through 14, 2020.
Copyright © 2021 by the American Society of Plastic Surgeons
DOI: 10.1097/PRS.0000000000008631

Disclosure: *The authors have no disclosures.*

Related digital media are available in the full-text version of the article on www.PRSJournal.com.

This work was supported by THE PLASTIC SURGERY FOUNDATION.

Copyright © 2021 American Society of Plastic Surgeons. Unauthorized reproduction of this article is prohibited.

clearance of radionucleotide tracer from the injection site and/or quantifies the accumulation of tracer in draining lymph nodes.[2,3] This technique is limited by variation in injection site used, choice and volume of radiotracer injected, and differences in imaging acquisition times.[2,4] In addition, it cannot be readily applied intraoperatively and has been found to yield unreliable results across human studies.[2,5,6]

Animal models designed to quantify lymphatic flow have been described. In 2009, Tobbia et al. quantified real-time lymphatic transport using a sheep model.[7] In their study, lymphatic flow was directly quantified after excision of a popliteal lymph node by monitoring the clearance of a radiolabeled albumin tracer at serial time points from a central venous line.[7] Despite encouraging results, this study is not readily clinically translatable, as it, again, uses nuclear dyes, which are difficult to implement in the clinical setting. In 2018, Tran et al. described a swine model to evaluate the lymphatic clearance of U.S. Food and Drug Administration–approved fluorophores.[8] The authors were able to directly quantify lymphatic clearance in real time after inguinal hindlimb lymphadenectomy and lymphadenectomy with immediate lymphovenous bypass or immediate lymphatic reconstruction.[9]

Although this animal paradigm was the first to provide objective data on lymphatic clearance using optical imaging, the model was not poised for direct clinical translation, as it required invasive measures such as direct cannulation of lymphatic vessels for dye injection, placement of a central venous line, and high volumes of dyes to reach sufficient blood levels for subsequent serum analyses. We intended to refine this established model,[8] with the aim of future clinical translation.

In this study, we introduce a large-animal model designed to directly quantify real-time lymphatic flow after lymphadenectomy and lymphovenous bypass. As immediate lymphatic reconstruction continues to gain acceptance[10] and broaden in its application, it is essential to develop a clinically translatable model conducive to further studies aimed at evaluating the technique in different experimental settings. We believe this study serves as a critical springboard in this effort.

METHODS

Animal Preparation

Ten female Yorkshire pigs (Parsons EM & Sons, Inc., Hadley, Mass.) with a mean weight of 30.0 ± 1.8 kg and average age of 3 to 4 months were used in this study. The experimental setup is demonstrated in Figure 1. A central venous catheter was inserted into the internal jugular vein. Heart rate, blood oxygenation, and body temperature were closely monitored during the experiment. One superficial epigastric vein was dissected and cannulated caudal to the costal margin using a 24-gauge angiocatheter (BD Medical, Franklin Lakes, N.J.). The contralateral superficial epigastric vein was similarly dissected and exposed for real-time imaging. On completion of each experiment, animals were euthanized.

Dye Preparation

To design near-infrared fluorescent agents with prolonged half-lives, we purchased purified human serum albumin from Sigma-Aldrich (St. Louis, Mo.) and conjugated it with ZW700-1C and ZW800-1 to produce ZW700–human serum albumin and ZW800–human serum albumin,

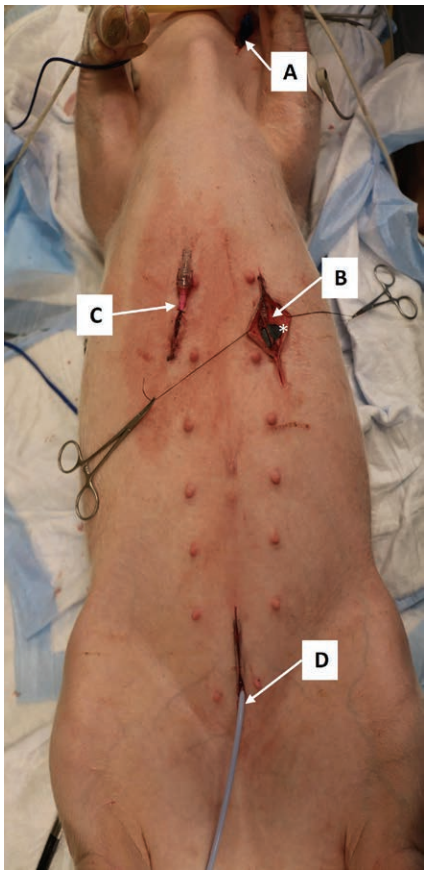

Fig. 1. Pig experimental setup. (*A*) The *arrow* indicates the central line that was used to monitor pig vital parameters and central blood draws. (*B*) the exposed left superficial epigastric vein that was used for continuous vein imaging throughout the experiment. (*C*) The *arrow* points to the right superficial epigastric vein that was cannulated for peripheral blood draws. (*D*) Here, the *arrow* points to the urinary catheter that was placed to monitor urinary output.

Copyright © 2021 American Society of Plastic Surgeons. Unauthorized reproduction of this article is prohibited.

respectively. Briefly, 10 equivalents of ZW700-1C *N*-hydroxysuccinimide ester[11] or ZW800-1 *N*-hydroxysuccinimide ester[12] was added to the purified human serum albumin in phosphate-buffered saline at a pH of 7.8 and incubated for 3 hours to form a stable amide linkage. ZW700–human serum albumin and ZW800–human serum albumin were purified using gel filtration chromatography and P6 cartridges. The labeling ratio was calculated from the ratio of extinction coefficients between the human serum albumin and the near-infrared fluorophore. The optical spectra of ZW700–human serum albumin and ZW800–human serum albumin are seen in Figure 2.

Study Paradigm

We designed three different experiments to evaluate lymphatic clearance in different anatomical models (Fig. 3). Laterality of injection site and lymphadenectomy (with or without lymphovenous bypass) were modified for each experiment. The control limb was used to obtain additional baseline clearance data.

1. In our first model, only baseline clearance curves were obtained. After induction and animal preparation, a 0.5-cc solution of hematoxylin was injected into each hindlimb. Then, 0.5 cc of ZW700–human serum albumin and ZW800–human serum albumin was injected intradermally into the left and right swine distal hindlimbs, respectively.
2. In our second model, a unilateral inguinal lymphadenectomy was performed. A lymphadenectomy was performed on one side, whereas no intervention was performed on the contralateral extremity.
3. In our third model, a unilateral inguinal lymphadenectomy was performed with an immediate lymphovenous bypass.

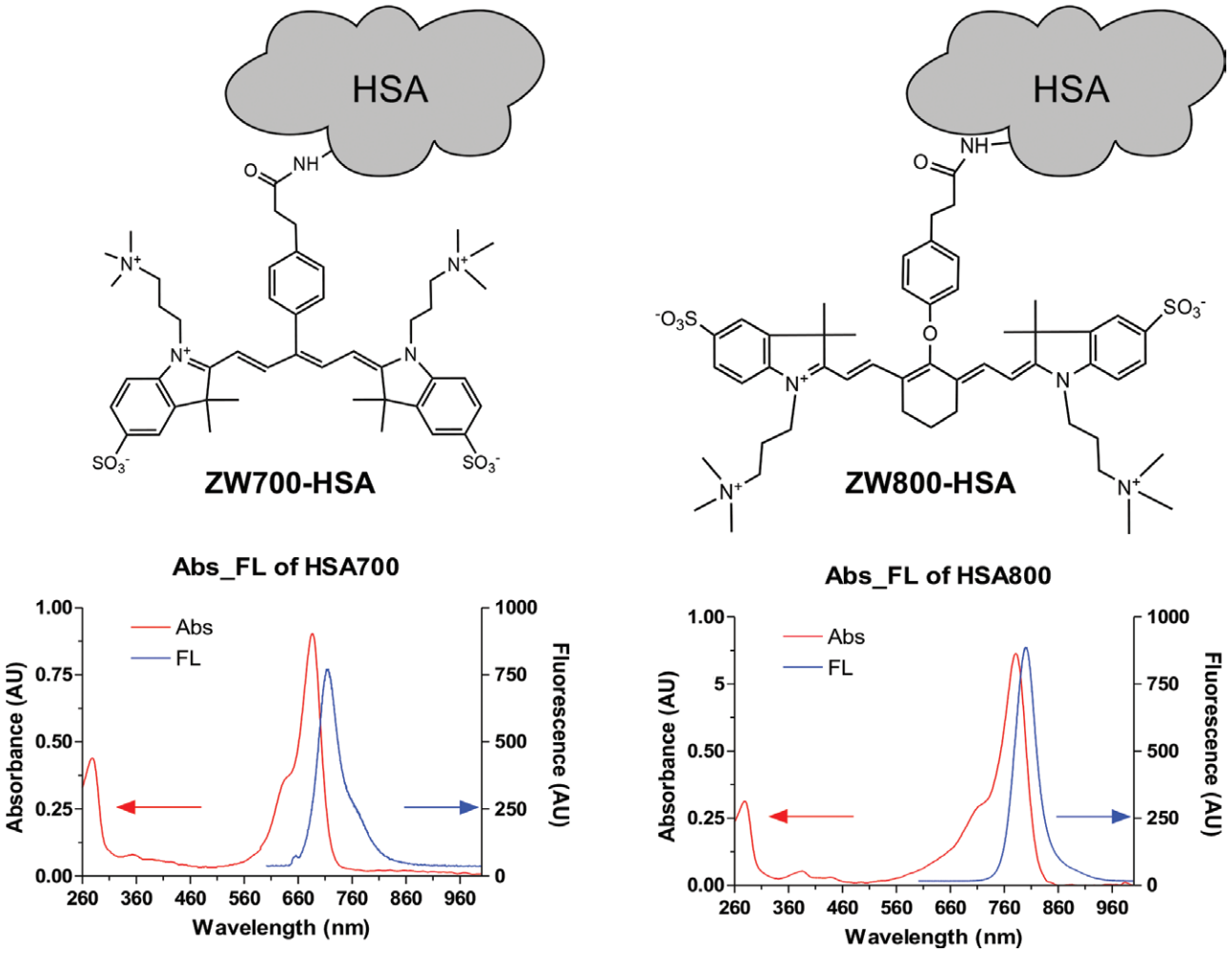

Fig. 2. ZW700–human serum albumin and ZW800–human serum albumin characteristics. The chemical composition of both dyes and their optical absorption and emissions spectrum is shown here.

Copyright © 2021 American Society of Plastic Surgeons. Unauthorized reproduction of this article is prohibited.

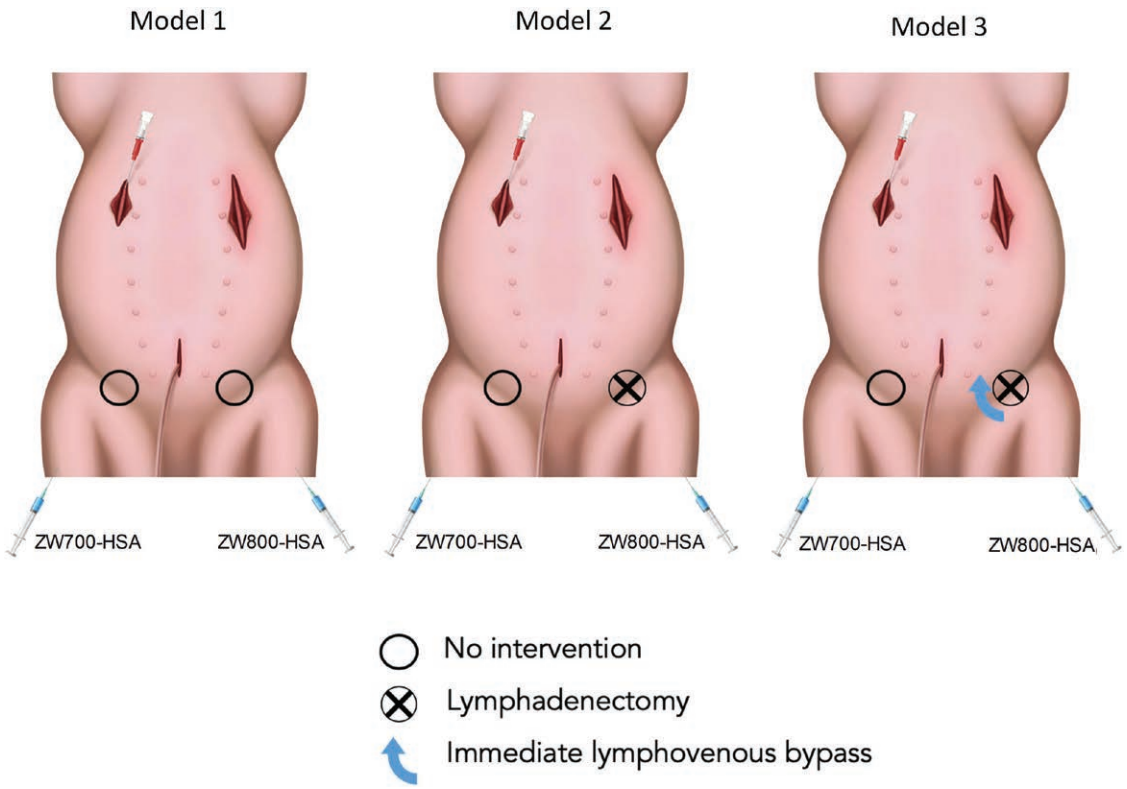

Fig. 3. Schematic depiction of the study paradigm. In model 1, baseline curves were obtained after injection of ZW700–human serum albumin and ZW800–human serum albumin (no intervention) dyes. In model 2, a unilateral lymphadenectomy was performed, and lymphatic clearance was quantified after dye injection. In model 3, lymphadenectomy with immediate lymphovenous bypass was performed and lymphatic clearance was then calculated.

In all three models, the injection sites were then massaged for 30 seconds to facilitate lymphatic flow. The left superficial epigastric vein and nearby skin on the torso were imaged throughout all experiments. Peripheral and central blood were drawn from the right superficial epigastric vein and central line at prescribed time intervals for subsequent analysis.

Intraoperative Imaging

Real-time imaging was conducted using a fluorescence-assisted resection and exploration[13] dual–near-infrared channel imaging system.[14–16] Briefly, the system provides two fluorescence excitation light sources shone on the target under the camera lens: a 660-nm and a 760-nm source, with (respectively) 1 mW/cm^2 and 3.6 mW/cm^2 flux intensities in the center of the field of view. The system's camera has three channels, providing simultaneous image capture for color, 700-nm, and 800-nm near-infrared fluorescence images. Each near-infrared channel provides 10-bit resolution gray-scale quantitative raw images for postexperiment data quantification. The superficial epigastric vein dissected for imaging was placed in the center of the camera's field of view. Care was taken to maintain the subject immobile to minimize variations in the imaging quantification (maintain working distance, focus, and excitation light distribution). To capture images, we used a special mode to automatically record image sequences with different exposure durations and to control the excitation sources. The value best balancing sensitivity and dynamic range was then selected after the experiment for each near-infrared channel. To optimize quantification results, we prevented crosstalk from the ZW700–human serum albumin into the 780-nm channel by only enabling one excitation light source for each image through the same automation mode.

Serum Analyses

Central and peripheral blood samples were obtained at set time intervals after dye injection using heparinized tubes. All samples were maintained at 4°C until the time of analysis. Blood

Copyright © 2021 American Society of Plastic Surgeons. Unauthorized reproduction of this article is prohibited.

samples were centrifuged, and the collected serum was placed in glass capillary tubes. To estimate the dye concentration in blood samples, a set of calibrated capillary tubes with predetermined concentrations were prepared from stock dye solutions, along with a control glass capillary tube with only serum.

The capillary tubes for each experiment were imaged with an in-house near-infrared system similar to the fluorescence-assisted resection and exploration.[13,17] The capillary tubes were placed in the center of the field of view. Capillary tubes were iteratively positioned using a template to ensure nearly identical position under the excitation light and minimize quantification errors. With only one excitation laser source active at a time, images for both excitation wavelength and each capillary tube were captured. Images were captured using an automated script to obtain sets with various exposure times, with 1000 msec providing the best balance between sensitivity and dynamic range.

Data Quantification

Blood Samples

Quantification of the data was performed using ImageJ software (National Institutes of Health, Bethesda, Md.).[18] For each capillary tube image set for the selected exposure time, a region of interest was drawn around a section containing the serum sample (Fig. 4). The same region of interest was used for a given set of capillary tube images (blood samples and calibrated set). The mean of the region in all images was extracted and saved for further analyses.

To mitigate background influence from either the camera or the imaging environment, the signal was quantified using a signal-to-background (SBR) ratio calculation:

$$SBR = \frac{I_s - I_0}{I_0} \quad (1)$$

where I_s is the signal intensity in a time point sample (mean in the region of interest), and I_0 is the signal from a sample taken before dye injection (background emissions without dye). The data are then plotted against time, and the slope represents the lymphatic clearance rate. The slope was extracted from the curves using a linear fit and is expressed as signal-to-background ratio. In this study's case, the units are milli–signal-to-background ratio per minute. To recover an indirect estimate of dye concentration, the signal-to-background ratio from the blood samples were scaled with the signal-to-background ratio from the calibrated set. However, figures are expressed in signal-to-background ratio for uniformity with real-time imaging.

Real-Time Imaging

Quantification extraction from the real-time images were also performed using the ImageJ software.[18] A region of interest was drawn around the exposed vein, and another region of interest was drawn over an area of normal skin (Fig. 5). The mean value of both regions of interest for each image set was extracted and stored. We attempted to minimize inadvertent pig movement to promote standardization of imaging parameters and limit changes in imaging conditions. Furthermore, two individuals performed all intraoperative imaging, limiting interrater variability.

As in the previous section, Equation 1 was applied to the data to mitigate background influence and slopes extracted from the data points. I_s is the signal mean from an region of interest in a time point image, and the I_0 value is the same

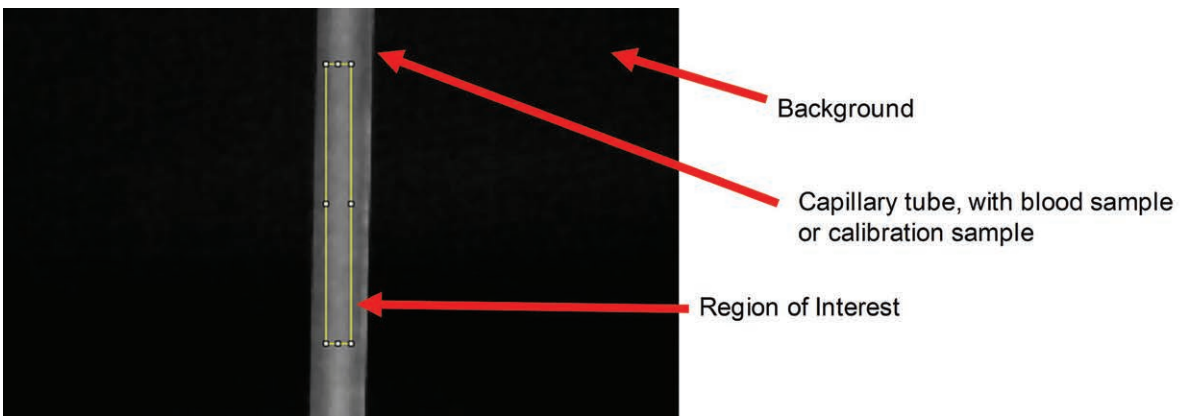

Fig. 4. Quantification of blood data. A region of interest is drawn over the center of the capillary tube containing a blood sample. An image from a tube with dye-free blood is used as I_0 for Equation 1.

Copyright © 2021 American Society of Plastic Surgeons. Unauthorized reproduction of this article is prohibited.

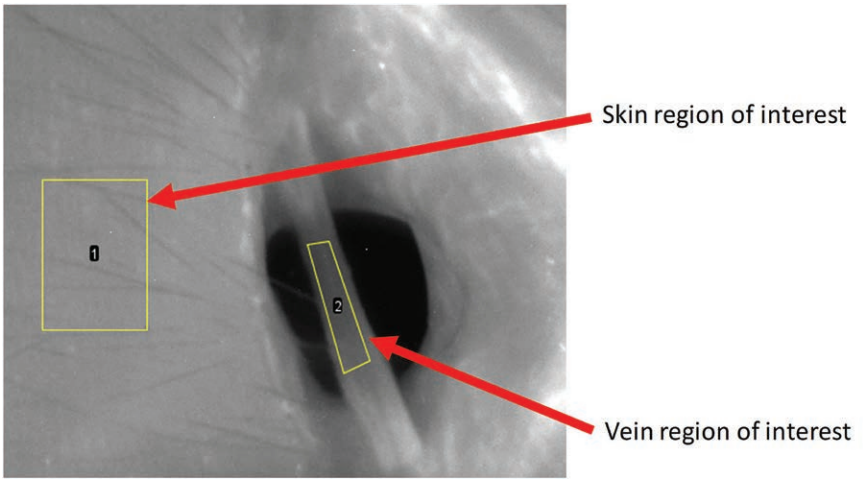

Fig. 5. Quantification of real-time skin and vein imaging. A region of interest is drawn over the vein and a defined area of skin. Involuntary animal manipulation requires minor but essential adjustments to the vein region of interest, because a few millimeters' offset will strongly affect the mean value. Skin is less prone to this impact because of the large available area and similar dye update in neighboring skin.

region of interest but from a reference image taken before dye injection, accounting for tissue autofluorescence.

RESULTS

Dye Concentration and Quantification Capability

Preliminary experimental trials showed no signal with 0.75 μmol of injected ZW700–human serum albumin and a very weak signal for 0.75 μmol of injected ZW800–human serum albumin for both real-time imaging and quantification in blood samples. The dose was therefore increased to 6.4 μmol for ZW700–human serum albumin and to 8.5 μmol for ZW800–human serum albumin in the 10 experiments conducted during this study. However, at 8.5-μmol concentration, the ZW800–human serum albumin signal was detected only slightly above background levels, making quantification attempts for this dye in serum, vein, and skin imaging inconclusive.

Similarly, the signal for ZW700–human serum albumin in the blood samples were detected only slightly above background levels. However, ZW700–human serum albumin provided sufficient signal above background levels during real-time imaging of the vein and skin to visualize and quantify lymphatic clearance except in two experiments. In one case, no signal was obtained, and these data were excluded from analysis and figures. Similarly, in a second case, the dye had degraded before injection, and those data were excluded. For this second case, data are shown in orange curves. [**See Figure, Supplemental Digital Content 1**, which shows lymphadenectomy with lymphovenous bypass venous imaging clearance curve. There was more variability in lymphovenous bypass curves using vein imaging. However, the concentration of dye on completion of the experiment is almost identical to that of the control curve. The vein diameter in experiment 7 (*orange*) had significant variations, suggesting uneven blood flow during the experiment and likely lower than with other experiments, explaining the nearly absent response of the dye in this figure, ***http://links.lww.com/PRS/E762***. **See Figure, Supplemental Digital Content 2**, which shows lymphadenectomy with lymphovenous bypass imaging skin imaging clearance curve. Clearance curves for lymphadenectomy with immediate lymphovenous bypass experiments are depicted. There is minimal variation between most experiments. Both control and lymphadenectomy with lymphovenous bypass curves reach similar final concentrations on completion of the experiment (t = 180 minutes). For experiment 7, whereas the dye had degraded, skin imaging still shows an early peak consistent with other experiments, although with a much-reduced amplitude, ***http://links.lww.com/PRS/E763***.]

Surgical Results

In all experiments where a lymphadenectomy was performed, imaging of the respective hindlimb of the draining lymphosome demonstrated cessation of flow at the lymphadenectomy

Copyright © 2021 American Society of Plastic Surgeons. Unauthorized reproduction of this article is prohibited.

site. For experiments where a lymphadenectomy with lymphovenous bypass was performed, anastomotic patency was confirmed in all experiments. [**See Figure, Supplemental Digital Content 3**, which shows molecular imaging of lymphovenous anastomotic site. This intraoperative image shows a successful lymphovenous bypass as the dye flows through the patent anastomotic site of the lymphovenous bypass. A failed bypass would instead show the dye spilling in the surgical cavity, ***http://links.lww.com/PRS/E764***. **See Video 1 (online)**, which shows real-time dye visualization of bypass patency shortly after injection. Dye can be visualized coursing through the lymphatic channel and through the patent anastomotic site of the lymphovenous bypass.] Of note, an anastomotic leak was observed in one experiment. The venous and skin imaging from this experiment did not demonstrate any increase in signal-to-background ratio and therefore these data were removed from the analysis. Therefore, we will report on our results using real-time venous and skin imaging after injection of ZW700–human serum albumin dye in seven experiments.

Vein Imaging

In each experiment, the superficial epigastric vein was dissected and exposed. The baseline curves demonstrate a mean constant clearance rate after 25 minutes (Fig. 6), with a slope of 7.4 milli–signal-to-background ratio units per minute. In experiments where a unilateral lymphadenectomy was performed, the mean clearance rate was 2.17 milli–signal-to-background ratio units per minute (Fig. 6), a 70 percent decrease from baseline. When a lymphovenous bypass was performed immediately after lymphadenectomy, the mean lymphatic clearance rate was 5.25 milli–signal-to-background ratio units per minute (Fig. 6), 30 percent less than at baseline. This is demonstrated in real time using a time-lapse video of venous imaging shortly after injection. [**See Video 2 (online)**, which shows real-time vein imaging. In this time-lapsed image, one can visualize the increased signal early in the experiment, consistent with rapid uptake from the lymphatics to the central circulation.] In the first 15 minutes of each experiment involving a successful lymphovenous bypass, there was a sharp increase in signal-to-background ratio (Fig. 6). Individual and mean experimental results for vein imaging can be seen. [**See Figure, Supplemental Digital Content 1**, ***http://links.lww.com/PRS/E762***. **See Figure, Supplemental Digital Content 4**, which shows lymphadenectomy venous imaging clearance curve. The lymphadenectomy clearance

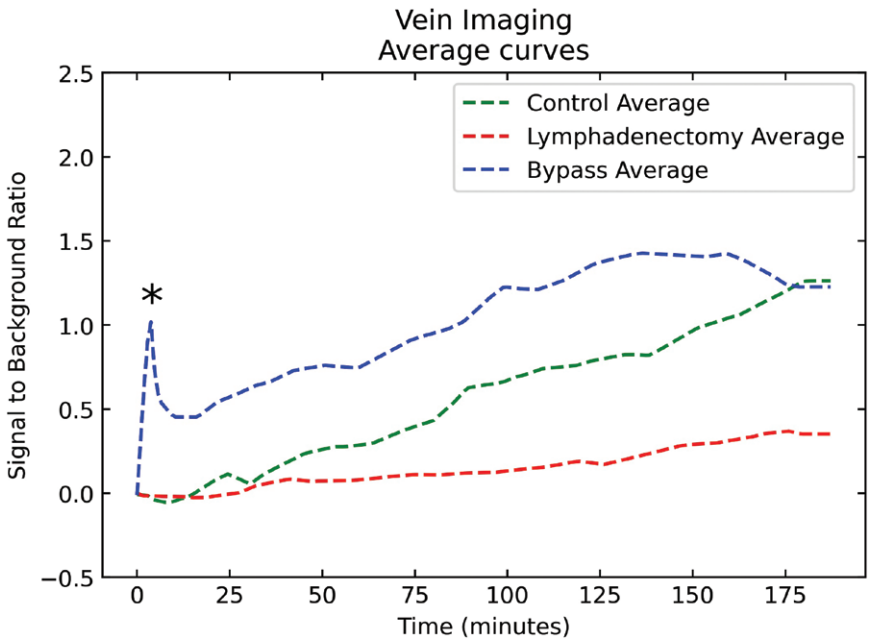

Fig. 6. Vein molecular imaging mean clearance curves. The mean clearance curves for vein imaging after lymphovenous bypass, lymphadenectomy, and control experiments are depicted. The *asterisk* reflects the initial uptick in molecule concentration, consistent with rapid uptake from the lymphatics to the central circulation. The mean molecule concentration reaches the control average at the end of the study (t = 180 minutes).

Copyright © 2021 American Society of Plastic Surgeons. Unauthorized reproduction of this article is prohibited.

curves were consistent across experiments and there was a significant decrease in clearance after lymphadenectomy (*red*) compared to control (*green*), ***http://links.lww.com/PRS/E765***.]

Skin Imaging

Baseline clearance curves showed a gradual increase in signal-to-background ratio as the experiments elapsed (Fig. 7). Results for all skin imaging experiments can be seen (**see Figure, Supplemental Digital Content 1**, ***http://links.lww.com/PRS/E762***). The control experiments have constant dye concentration increase, with an average slope of 10.2 milli–signal-to-background ratio units per minute (Fig. 7). After lymphadenectomy, the slope reduced to 2.7 milli–signal-to-background ratio units, a 74 percent decrease from baseline (Fig. 7). When a lymphovenous bypass was performed after lymphadenectomy, the slope decreased by only 25 percent, reaching 7.6 milli–signal-to-background ratio units per minute (Fig. 7). The slopes from skin imaging were noted to be smoother than with venous imaging. We noticed an initial spike in molecule concentration, correlating with a sharp increase in the mean slope (Fig. 7) during the first 10 minutes of the experiment. An intraoperative image depicting skin and vein imaging locations is seen in Figure 8. The generation of clearance curves using both imaging modalities, based on real-time changes in signal-to-background ratio, is shown in Figure 9.

DISCUSSION

In this study, we aimed to develop a more clinically translatable animal model using a novel protocol to assess lymphatic clearance in real time using noninvasive molecular imaging. To date, quantification of lymphatic clearance has been largely evaluated by invasive means, which requires direct cannulation of peripheral lymphatics, serial blood draws obtained from a central line, and use of nuclear dyes. Our study has three key findings. First, noninvasive vein and skin molecular imaging demonstrate consistent results for quantifying lymphatic flow. Second, although vein and skin imaging demonstrated concordance, skin imaging results were more consistent. Finally, although our results are encouraging, there is a need to refine the dye concentration of our fluorophores to optimize molecular imaging in blood samples.

Regardless of quantification challenges, a key finding in our study was the ability to use small

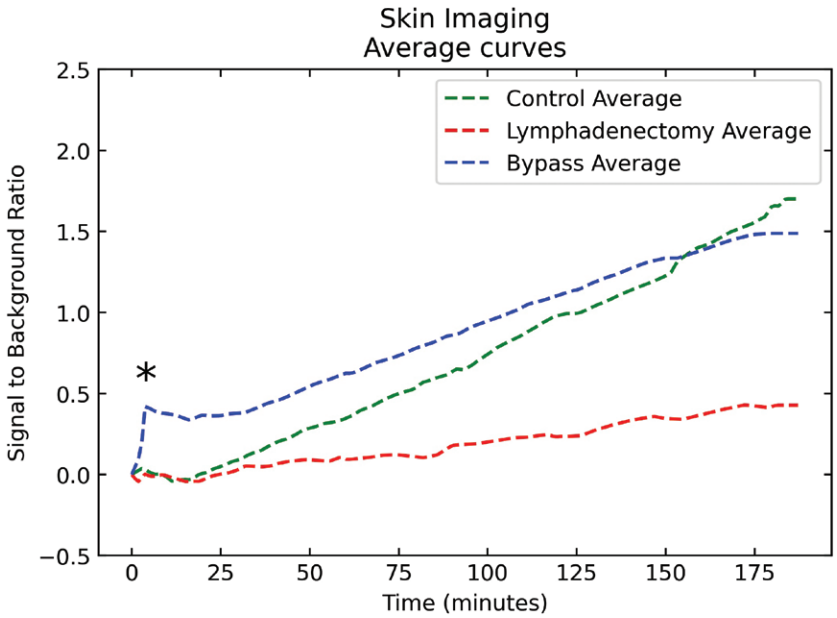

Fig. 7. Skin molecular imaging mean clearance curves. The mean curves for skin imaging after lymphovenous bypass, lymphadenectomy, and control experiments are depicted. The mean curves are more consistent than those for vein imaging across all three experimental scenarios. Again, the *asterisk* depicts the initial rapid uptake of molecule concentration after bypass completion, which is also seen in vein imaging. The molecule concentration for bypass experiments is similarly almost equivalent to control experiments at $t = 180$ minutes.

Copyright © 2021 American Society of Plastic Surgeons. Unauthorized reproduction of this article is prohibited.

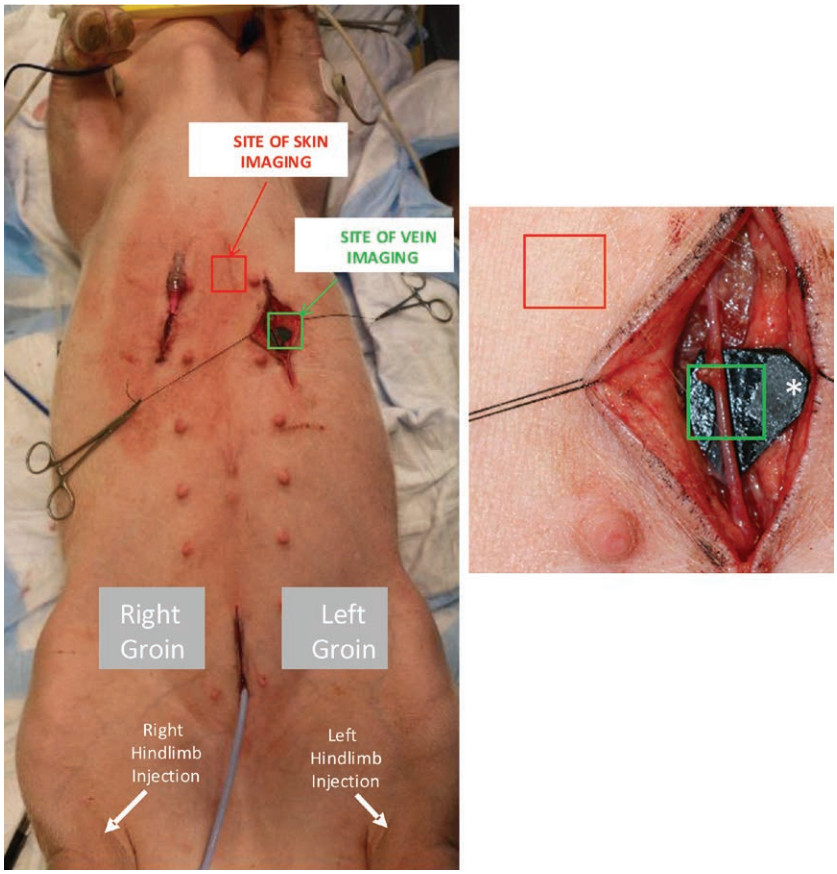

Fig. 8. Real-time skin and vein imaging. The sites of injection and skin and venous imaging are shown (*left*). A closer view at these two sites is shown (*right*). The *asterisk* indicates the location of the black background used for vein imaging.

volumes of optically active, clinically applicable dyes injected intradermally to evaluate clearance. Currently, the gold standard for assessment of lymphatic flow and drainage patterns involves lymphoscintigraphy, which requires nuclear dyes and exposes patients to ionizing radiation.[19] Furthermore, agents commonly used for lymphoscintigraphy have unpredictable absorption patterns and transit times, limiting their ability to accurately and reliably quantify lymphatic clearance in real time.[2] Vein and skin optical imaging both demonstrated a drop in lymphatic clearance after lymphadenectomy. This decrease was mitigated when an immediate lymphovenous bypass was performed. Furthermore, the initial spike after lymphovenous bypass was observed in both skin and venous imaging, supporting rapid uptake of the dye from the lymphatics into the central circulation (i.e., shorter transit times). The concentration decreased as the initial dose was diluted throughout the vasculature system and then returned to a constant increase, with slopes similar to the baseline experiments.

Acknowledging that these experiments were performed using an animal paradigm, we believe our findings may have powerful clinical applications. For example, interest in performing an immediate lymphovenous bypass at the time of lymphadenectomy continues to grow in tandem with promising clinical results demonstrating decreases in postoperative lymphedema in high-risk patient cohorts.[10,20,21] Given our current findings, the quantification of molecular clearance could serve as an individualized marker for an upper extremity's lymphatic clearance in patients undergoing nodal intervention. This value would not only provide the treating clinician with real-time, individualized knowledge of patient lymphatic function, but could also inform management (e.g., the potential need to perform lymphovenous bypass), evaluate intraoperative patency, and guide postoperative surveillance.

Another key finding from our study is that skin imaging revealed more time-consistent results compared to vein imaging. Specifically, we noted more variability in vein signal-to-background ratio

Copyright © 2021 American Society of Plastic Surgeons. Unauthorized reproduction of this article is prohibited.

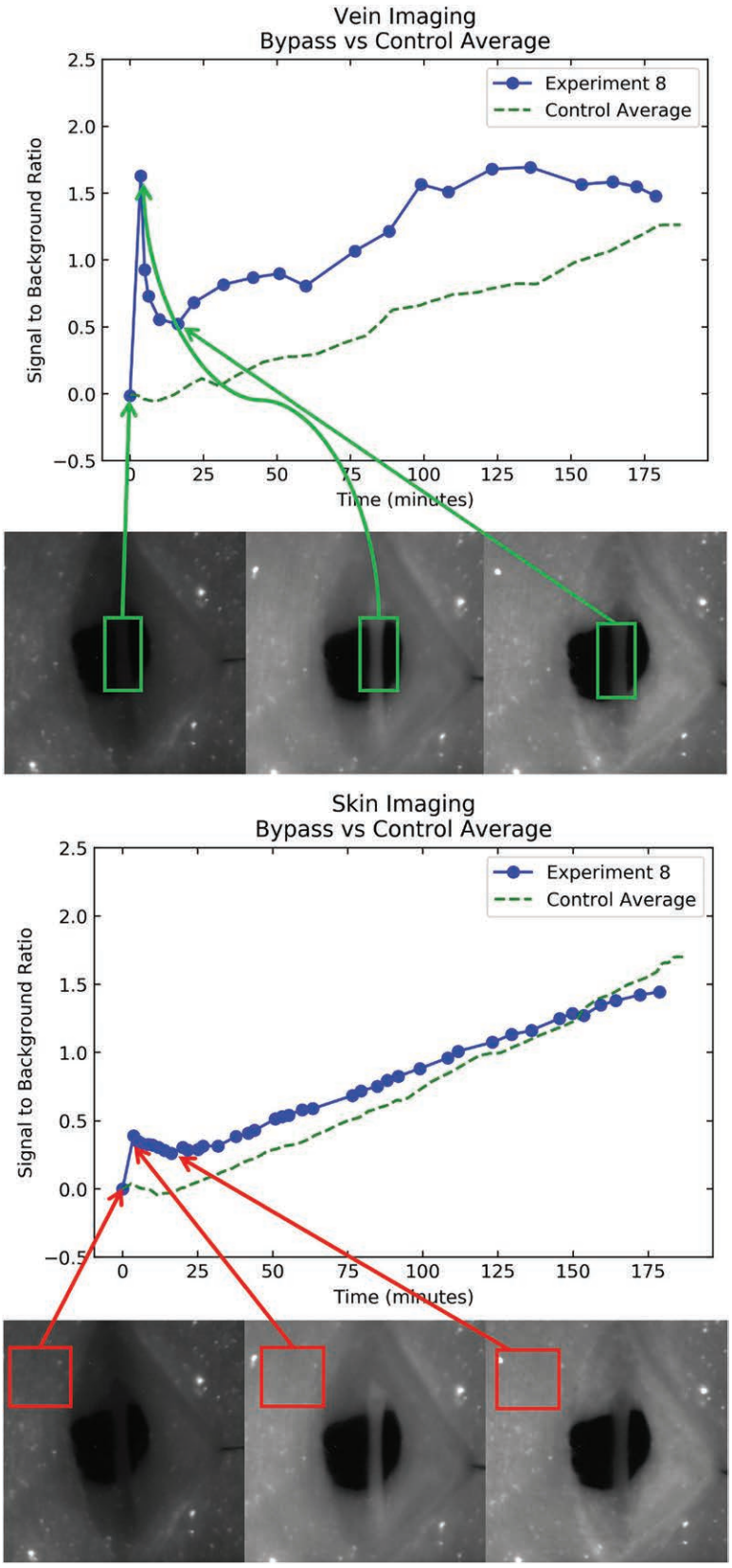

Fig. 9. Real-rime clearance curves. Here, one can see the generation of clearance curves in real time using both vein (*above*) and skin imaging (*below*). At 3 minutes, one can appreciate the initial spike in signal-to-background ratio in both *above* and *below*, denoted by an *asterisk*, suggestive of quick uptake from the lymphatic to the venous system using both imaging modalities.

Copyright © 2021 American Society of Plastic Surgeons. Unauthorized reproduction of this article is prohibited.

curves than skin imaging curves, which demonstrated smoother slopes (Figs. 8 and 9). We hypothesize that this finding is attributable to two factors. First, the distribution of the excitation light is generally not uniform and can vary up to 10 percent. Thus, when the vein inadvertently moves into a different illuminated area during the experiment, it will invariably affect the quantification. Skin imaging, in contrast, was not affected by movement, as neighboring skin can be expected to have similar dye concentrations. The region of interest needs to be drawn only once and simultaneously extracted from all images, greatly simplifying data processing. In addition, this noninvasive approach is more amenable to clinical translation and may hold the promise of providing valuable information regarding lymphatic function during clinical procedures for patients undergoing nodal extirpation.

Our final key finding is the need to further refine dye concentrations. Although noninvasive imaging was possible with ZW700–human serum albumin, we were unable to accurately quantify clearance from blood samples. For ZW700–human serum albumin, we hypothesize that our small blood sample quantities limited our ability to detect any signal. In the future, we will use larger volumes of blood and larger diameter capillary tubes to effectively increase quantification sensitivity. For ZW800–human serum albumin, preliminary real-time experiments indicated the need to increase our dye concentration. Unfortunately, higher dye concentrations resulted in considerable dye aggregation, causing a significant reduction in signal. The total dose and injection volume must then be optimized to increase the observable signal in future experiments.

There are inherent limitations in our study design. Our experimental animal model was a nonsurvival model, precluding any ability to monitor any long-term changes in lymphatic function after lymphadenectomy and lymphadenectomy with lymphovenous bypass over time. We are therefore unable to draw conclusions between lymphatic clearance rates and any potential correlations with development of lymphedema. Our nonsurvival study would not provide the ability to analyze whether or not clearance would improve beyond 3 hours. This emphasizes the need to conduct a survival model to monitor animals postoperatively for lymphedema detection. In addition, there is no widely accepted animal model for lymphedema. To that end, we feel that the swine model is an excellent model because the lymphatics most closely resemble those of humans. However, the purpose of this study was not to assess lymphedema development, but rather to develop and validate a methodology to assess real-time lymphatic clearance using novel fluorophore and imaging technology. Furthermore, the dyes used require additional evaluation and study in humans before broadened application can be considered.

Moreover, unlike for blood samples which can be compared against calibrated samples, for real-time molecular imaging of the skin, we were able to provide only relative trends. Varying skin tone between patients will also cause numeric values to change, so the noninvasive imaging technique might not truly capture the bypass's efficacy or stability over time. There is a need to evaluate this technique in animals of different skin color to assess reproducibility and ultimately broaden the application of this approach. Moving forward, survival studies would facilitate the ability to evaluate how lymphatic clearance is affected by key lymphedema risk factors, including radiation therapy.

CONCLUSIONS

In this study, we were able to demonstrate the feasibility of using noninvasive skin imaging as a method to detect lymphatic molecular clearance. This model can serve as a springboard for further investigation of the utility of molecular imaging to noninvasively quantify molecular clearance in different surgical and nonsurgical scenarios and evaluate its efficacy as a biomarker for lymphatic function.

Dhruv Singhal, M.D.
Division of Plastic and Reconstructive Surgery
Beth Israel Deaconess Medical Center
110 Francis Street, Suite 5A
Boston, Mass. 02215
dsinghal@bidmc.harvard.edu
Twitter: @drdhruvsinghal

ACKNOWLEDGMENTS

This work was funded by the Plastic Surgery Foundation, the American Society of Reconstructive Microsurgery, and the Lymphatic Education and Awareness Network. It was funded in part by the National Science and Engineering Research Council of Canada, the Banting Fellowship program, and U.S. National Institutes of Health grant NIBIB R01-EB022230. The authors would like to acknowledge Priyanka Das, Melisa D. Granoff, Christine O. Kang, Kate G. Park, Sheena Santos, and Wesley Stiles for contributions to this study.

REFERENCES

1. Yuan Z, Chen L, Luo Q, Zhu J, Lu H, Zhu R. The role of radionuclide lymphoscintigraphy in extremity lymphedema. *Ann Nucl Med.* 2006;20:341–344.

Copyright © 2021 American Society of Plastic Surgeons. Unauthorized reproduction of this article is prohibited.

2. Szuba A, Shin WS, Strauss HW, Rockson S. The third circulation: Radionuclide lymphoscintigraphy in the evaluation of lymphedema. *J Nucl Med.* 2003;44:43–57.
3. O'Donnell TF Jr, Rasmussen JC, Sevick-Muraca EM. New diagnostic modalities in the evaluation of lymphedema. *J Vasc Surg Venous Lymphat Disord.* 2017;5:261–273.
4. Forte AJ, Boczar D, Huayllani MT, Lu X, Ciudad P. Lymphoscintigraphy for evaluation of lymphedema treatment: A systematic review. *Cureus* 2019;11:e6363.
5. Partsch H. Assessment of abnormal lymph drainage for the diagnosis of lymphedema by isotopic lymphangiography and by indirect lymphography. *Clin Dermatol.* 1995;13:445–450.
6. Mihara M, Hara H, Araki J, et al. Indocyanine green (ICG) lymphography is superior to lymphoscintigraphy for diagnostic imaging of early lymphedema of the upper limbs. *PLoS One* 2012;7:e38182.
7. Tobbia D, Semple J, Baker A, Dumont D, Semple A, Johnston M. Lymphedema development and lymphatic function following lymph node excision in sheep. *J Vasc Res.* 2009;46:426–434.
8. Tran BNN, Angelo JP, Lee JH, et al. A novel pilot animal model for the surgical prevention of lymphedema: The power of optical imaging. *J Surg Res.* 2018;221:285–292.
9. Johnson AR, Singhal D. Immediate lymphatic reconstruction. *J Surg Oncol.* 2018;118:750–757.
10. Agarwal S, Garza RM, Chang DW. Lymphatic microsurgical preventive healing approach (LYMPHA) for the prevention of secondary lymphedema. *Breast J.* 2020;26:721–724.
11. Hyun H, Henary M, Gao T, et al. 700-nm zwitterionic near-infrared fluorophores for dual-channel image-guided surgery. *Mol Imaging Biol.* 2016;18:52–61.
12. Choi HS, Nasr K, Alyabyev S, et al. Synthesis and in vivo fate of zwitterionic near-infrared fluorophores. *Angew Chem Int Ed Engl.* 2011;50:6258–6263.
13. Lee BT, Hutteman M, Gioux S, et al. The FLARE intraoperative near-infrared fluorescence imaging system: A first-in-human clinical trial in perforator flap breast reconstruction. *Plast Reconstr Surg.* 2010;126:1472–1481.
14. Tanaka E, Choi HS, Fujii H, Bawendi MG, Frangioni JV. Image-guided oncologic surgery using invisible light: Completed pre-clinical development for sentinel lymph node mapping. *Ann Surg Oncol.* 2006;13:1671–1681.
15. Choi HS, Ashitate Y, Lee JH, et al. Rapid translocation of nanoparticles from the lung airspaces to the body. *Nat Biotechnol.* 2010;28:1300–1303.
16. Kim SH, Park G, Hyun H, et al. Near-infrared lipophilic fluorophores for tracing tissue growth. *Biomed Mater.* 2013;8:014110.
17. Gioux S, Kianzad V, Ciocan R, Gupta S, Oketokoun R, Frangioni JV. High-power, computer-controlled, light-emitting diode-based light sources for fluorescence imaging and image-guided surgery. *Mol Imaging* 2009;8:156–165.
18. Rueden CT, Schindelin J, Hiner MC, et al. ImageJ2: ImageJ for the next generation of scientific image data. *BMC Bioinformatics* 2017;18:529.
19. Alazraki N, Glass EC, Castronovo F, Olmos RA, Podoloff D; Society of Nuclear Medicine. Procedure guideline for lymphoscintigraphy and the use of intraoperative gamma probe for sentinel lymph node localization in melanoma of intermediate thickness 1.0. *J Nucl Med.* 2002;43:1414–1418.
20. Boccardo F, Casabona F, De Cian F, et al. Lymphatic microsurgical preventing healing approach (LYMPHA) for primary surgical prevention of breast cancer-related lymphedema: Over 4 years follow-up. *Microsurgery* 2014;34:421–424.
21. Hahamoff M, Gupta N, Munoz D, et al. A lymphedema surveillance program for breast cancer patients reveals the promise of surgical prevention. *J Surg Res.* 2019;244:604–611.

Copyright © 2021 American Society of Plastic Surgeons. Unauthorized reproduction of this article is prohibited.